A novel structure to enhance magnetic force and velocity in tubular linear reluctance motor

Ali MOSALLANEJAD*, **Abbas SHOULAIE**
Electrical Engineering Department, Iran University of Science and Technology,
Narmak, Tehran-IRAN
e-mails: mosallanejad@iust.ac.ir, shoulaie@iust.ac.ir

Abstract

In this paper, a novel design for a tubular linear reluctance motor (TLRM) has been developed. This paper presents a novel structure to enhance magnetic force and velocity in a TLRM. The new structure is accomplished through some changes in a TLRM, which results in a step winding structure. Comparing the proposed motor and the typical motor performances, it is proven that the proposed motor has better performance. For dynamic modeling of the proposed TLRM and to obtain the motor output characteristics, the method used for inductance profile calculation is described. The performance improvements in the proposed motor are evaluated using experimental results and finite element method analysis. At the end, the simulation results are compared with the experimental ones. Good agreement between the experimental and simulation results is observed.

Key Words: *Tubular linear reluctance motors, reluctance accelerator, step winding, high-speed actuator, finite element method analyses*

1. Introduction

Linear motors provide the solution to a wide variety of industrial needs, ranging from jackhammers to photolithography [1-5]. The switched reluctance (SR) motor is an old member of the electrical motor family. The first SR motor can be traced back to the early 19th century [6]. The main advantages of SR motors are their simple structure, ruggedness, and the fact that they are relatively inexpensive to manufacture. The linear reluctance motor is a linear motor that is considered under both AC and DC supply. Although AC motors have lower efficiency than DC motors, they are utilized in many applications [7]. Linear motors differ in both construction and type. One of the known motors in the group of linear motors is the tubular linear reluctance motor (TLRM), which can operate in different modes, such as the self-oscillating mode, switched-oscillating mode, and accelerator mode. A TLRM consists of 2 main parts: a moving part and a stator. The stator is composed of an exciting coil that produces the magnetic field, while the moving part is a ferromagnetic material called a plunger. A TLRM in its simplest form is presented in Figure 1 [7,8].

---

*Corresponding author: Electrical Engineering Department, Iran University of Science and Technology, Narmak, Tehran-IRAN
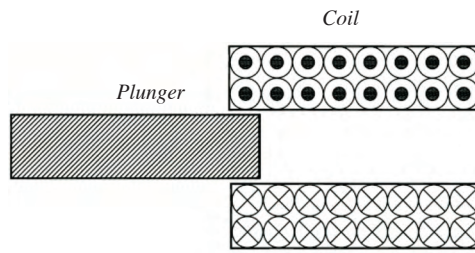
Figure 1. TLRM with an open magnetic system.

A TLRM is an electric motor in which velocity and magnetic force are produced by the tendency of its movable part (plunger) to move to a position where the inductance of the excited winding is maximized or, in other words, the reluctance to magnetic flux is minimized. Ferromagnetic material in the plunger reduces the reluctance and, therefore, magnetic force is developed due to the change in the reluctance of the material surrounding the coil as the plunger moves. The ferromagnetic plunger has a greater magnetic permeability than the air it replaces. As a consequence, the magnetic flux can be formed more easily when the plunger is centered in the coil. At this point, the reluctance is at its minimum for a given flux level; it is also the position of the least energy. When displaced from the centered position, magnetic forces will always act in a way to restore the plunger to its centered position. The TLRM is a series of coils activated sequentially to pull the plunger along the bore. Note that the plunger is only pulled; it is never pushed. This is a disadvantage of the TLRM when compared with other synchronous accelerators that can push and pull by choosing the relative polarity of the armature and stator windings.

Tomczuk and Sobol [7] investigated TLRMs in various types of magnetic circuits. They analyzed the magnetic field and calculated the integral parameters of the field and, moreover, they determined static characteristics and electromagnetic parameters of the motor. In [8], the performance of the linear reluctance oscillating motor operating under AC and DC supply was also investigated. Reluctance accelerator design and the methods used in its design were described in [9], along with the control methods of the accelerator and their predicted performance. In [10], Mendrela demonstrated the design and principle of the operation and performance of a linear reluctance self-oscillating motor. That paper examined a mathematical model of a motor, permitting analysis of the dynamics and transients occurring in this circuit. An experimental method for the determination of the equivalent-circuit parameters of a tubular SR motor was presented in [11]. Moreover, in [12], an E-core interior permanent magnet linear oscillating actuator was analyzed theoretically and validated via experimental results. The coupled field-circuit model of the 3-stage reluctance accelerator was presented in [13]. Another paper studied the design features of variable air gap and cylindrical and variable reluctance actuators [14]. There are many papers about modeling and analyzing TLRMs in which different modes of operation were discussed [15]. In [16], a linear reluctance motor was analyzed utilizing the finite element method (FEM) in the accelerating mode. However, methods for increasing force and velocity were not sufficiently discussed. In this paper, a novel method for increasing force and velocity in TLRMs is given and further discussed.

In TLRMs, the force is proportional to the derivative of inductance. As a result, to increase the former, the slope of the inductance waveform must be increased. To obtain this goal, it is necessary to make some changes in the motor winding structure so that the slope of the inductance waveform is increased. In the present paper, a new TLRM structure for gaining the maximum inductance derivative is introduced and the inductance curve calculations are discussed. The new TLRM is modeled and compared with a typical TLRM in force, velocity, and efficiency, and, at the end, the method used for inductance calculation and modeling,

simulation, and experimental results are compared. Furthermore, the force produced with each TLRM is calculated and compared using FEM analysis.

2. Novel step winding structure

As discussed earlier, this method is based on increasing the slope of the inductance curve. Consequently, some changes must be made in the TLRM winding structure in order to increase the derivative of inductance. Figure 2 represents the inductance and its derivative for a motor with level winding and a length of 20 cm.
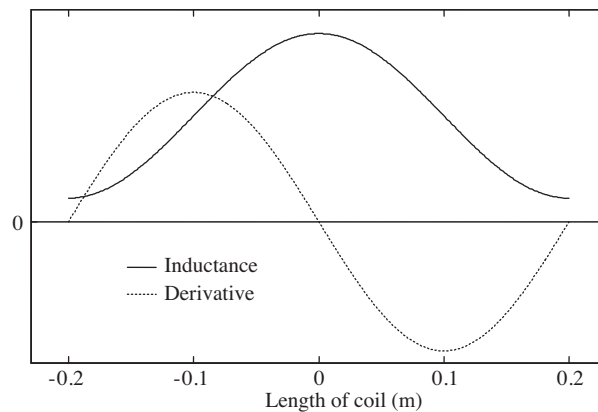

**Figure 2.** The inductance and the inductance derivative waveforms.

As can be seen, the inductance increases while the plunger enters the coil and reaches its maximum when placed completely inside the coil; however, the inductance decreases while the plunger exits the coil. The curve of the derivative shown in Figure 2 is proportional to the plunger position; at first the derivative increases and reaches its maximum, while half of the plunger is inside the coil, and then it decreases to 0 when the plunger is completely inside the coil. The same behavior can be seen when the plunger exits the coil. The higher the difference is between the maximum and minimum amount of inductance, the more the slope of the inductance curve increases and, therefore, the more the force increases. In this proposed method, the slope of the inductance is increased without changing the total winding turns. The main problem is where to increase the slope of the inductance. Experimental results show that if the plunger enters the coil with an initial velocity not equal to 0, motor efficiency and other motor output characteristics will improve. Consequently, we prefer to increase the slope of the inductance curve at the beginning of the winding so that it can function as an initial velocity. The winding structure should be changed to have the derivative of inductance increased at the beginning of the winding. Figure 3 shows the structure of a TLRM with level winding.

This motor's winding has N turns, which are divided into 6 different regions. The number of turns in each region is specified. To increase the inductance derivative at the beginning of the winding, the turn number for the winding in this region must be increased. As a result, the turns for the winding in the fifth region in Figure 3 are transferred to the top of the first region.

Figure 4 represents the changed winding structure of a TLRM, which is referred to as unlevel winding or step winding by the authors.

1065
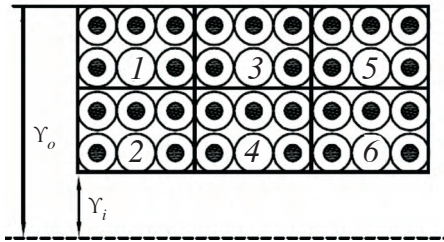
Figure 3. Schematic of the simplified level winding geometry.
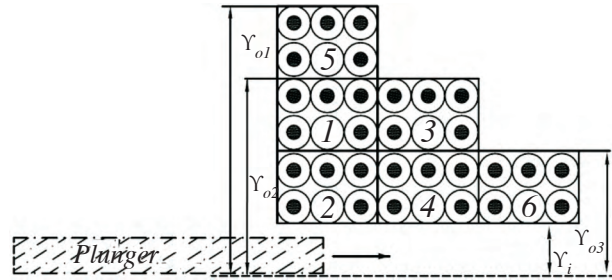
Figure 4. Schematic of the simplified step winding geometry.

In Figure 4, the windings are divided into 3 parts with similar length. The first part includes regions 1, 2, and 5. The second part includes regions 3 and 4, and, finally, the third part includes region 6. However, the number of windings and their lengths can be chosen differently.

3. Step winding inductance calculation

The magnetic force in a TLRM is derived from the following equation:

$$f_m = 0.5i^2 \frac{dL}{dx}. \tag{1}$$

In Eq. (1), the magnetic force is dependent on the derivative of inductance. Therefore, it is necessary to calculate the motor inductance as a function of the plunger position in the coil. The step windings of Figure 4 consist of 3 parts, which can be written shown below.

$$N = N_1 + N_2 + N_3 \tag{2}$$

$$L_{\min(T)} = L_{\min(1)} + L_{\min(2)} + L_{\min(3)} \tag{3}$$

$$L_{\max(T)} = L_{\max(1)} + L_{\max(2)} + L_{\max(3)} \tag{4}$$

Here, $L_{min(T)}$ is the minimum inductance of the step winding motor, $L_{max(T)}$ is the maximum inductance of the step winding motor, $L_{min(i)}$ is the minimum inductance of the ith parts of the step winding motor, and $L_{max(i)}$ is the maximum inductance of the ith parts of the step winding motor.

The parts of the winding shown in Figure 4 are so close to each other that there is a mutual inductance between them, and so in the calculated inductances, the mentioned mutual inductance is considered. In Eq. (2), N_1 is the ensemble winding turns for the first, second, and fifth regions; N_2 is the sum of the winding turns for the third and fourth regions; and N_3 is equal to the winding turns for the sixth region in Figure 4.

The previous equations indicate that the step winding consists of 3 separate virtual windings. In this method, an operation region is defined for each section. The winding inductance is only defined in its relevant region. The first virtual winding inductance that is defined in its relevant region, the first region, can be stated as follows:

$$L_1 = L_{m1} \left[1 + \cos\left(\frac{3\pi}{l}\left(\frac{2l}{3} - x\right)\right) \right] + L_{\min(T1)} \quad , -l < x < -\frac{2l}{3}, \tag{5}$$

in which L_{m1} and $L_{min(T1)}$ are defined as follows:

$$L_{m1} = \frac{L_{\max(1)} - L_{\min(1)}}{2},$$

(6)

$$L_{\min(T1)} = L_{\min(T)}.$$

(7)

Eq. (5) defines the inductance while the plunger is at the beginning of the coil until the time it reaches the end of the first winding. Consequently, the inductance is at its minimum ($L_{min(T1)}$) when the plunger is placed at the beginning of the first winding and reaches its maximum ($L_{max(T1)}$) when the plunger reaches the end of the first winding. The maximum inductance in the first virtual winding is equal to the sum of the maximum inductances of the first part and the minimum inductance of the second and third virtual windings. Very likely, the winding inductance in the second region is defined as in Eq. (8).

$$L_2 = L_{m2}\left[1 + \cos\left(\frac{3\pi}{l}\left(\frac{l}{3} - x\right)\right)\right] + L_{\min(T2)}, \qquad -\frac{2l}{3} < x < -\frac{l}{3}$$

(8)

In the above equation,

$$L_{m2} = \frac{L_{\max(2)} - L_{\min(2)}}{2}.$$

(9)

Eq. (8) calculates the motor winding inductance due to plunger movement from the beginning to the end of the second virtual winding. When the plunger is at the beginning of the second region, the inductance is at its minimum and can be calculated as follows:

$$L_{\min(T2)} = L_{\max(1)} + L_{\min(2)} + L_{\min(3)}.$$

(10)

The maximum inductance in the second region is equal to the sum of the maximum inductances of the first and second virtual windings and the minimum inductance of the third virtual winding. In addition, for the third virtual winding in its defined region, it can be stated that:

$$L_3 = L_{m3}\left[1 + \cos\left(\frac{3\pi}{l}\left(-x\right)\right)\right] + L_{\min(T3)}, \; -\frac{l}{3} < x < 0,$$

(11)

where:

$$L_{m3} = \frac{L_{\max(3)} - L_{\min(3)}}{2}.$$

(12)

Eq. (11) calculates the winding inductance with respect to the plunger movement from the end of the second virtual winding to the end of the third virtual winding. In the position where the plunger is at the beginning of the third virtual winding, the inductance is at its minimum and can be described as:

$$L_{\min(T3)} = L_{\max(1)} + L_{\max(2)} + L_{\min(3)}.$$

(13)

The maximum inductance is equal to the sum of the maximum inductance of the first, second, and third virtual windings. The calculated inductances above are for plunger movements from the beginning of the first virtual winding to the end of the third virtual winding in an unlevel winging motor with 3 steps when the plunger is about to enter the coil. If the plunger is exiting the coil, the above equations cannot be used to calculate the

inductance. If we have n steps instead of 3, the inductance in each part, while the plunger is passing through the part, can be described as follows:

$$L_i = L_{mi} \left[1 + \cos \left(\frac{n\pi}{l} \left(\frac{(n-i)\,l}{n} - x \right) \right) \right] + L_{\min(Ti)}, \quad -\frac{(n+1-i)\,l}{n} < x < -\frac{(n-i)\,l}{n}, \tag{14}$$

where:

$$L_{\min(Ti)} = \sum_{j=1}^{i-1} L_{\max(j)} + \sum_{j=i}^{n} L_{\min(j)}, \, i = 1, 2, \dots, n. \tag{15}$$

For L_{mi}, we have:

$$L_{mi} = \frac{L_{\max(Ti)} - L_{\min(Ti)}}{2}, \tag{16}$$

where:

$$L_{\max(Ti)} = \sum_{j=1}^{i} L_{\max(j)} + \sum_{j=i+1}^{n} L_{\min(j)}, \, i = 1, 2, \dots, n. \tag{17}$$

In the above equations, i is the number of the part in which the inductance is calculated. The inductance decreases when the plunger is about to exit the winding, which can be calculated as in Eq. (18) in a step winding motor with n steps.

$$L_i = L_{mi} \left[1 + \cos \left(\frac{n\pi}{l} \left(\frac{(i-1)\,l}{n} - x \right) \right) \right] + L_{\min(Ti)}, \qquad \frac{(i-1)\,l}{n} < x < \frac{il}{n} \tag{18}$$

In the above equation,

$$L_{\min(Ti)} = \sum_{j=1}^{i} L_{\min(j)} + \sum_{j=i+1}^{n} L_{\max(j)}, \, i = 1, 2, \dots, n, \tag{19}$$

$$L_{\max(Ti)} = \sum_{j=1}^{i-1} L_{\min(j)} + \sum_{j=i}^{n} L_{\max(j)}, \, i = 1, 2, \dots, n, \tag{20}$$

$$L_{mi} = \frac{L_{\max(Ti)} - L_{\min(Ti)}}{2}. \tag{21}$$

It should be mentioned here that the equations used for calculating the inductance when the plunger enters the coil and when it exits are different.

4. Dynamic modeling

Generally, the motor can operate either in a horizontal or vertical position. When it operates in a horizontal position, it is not necessary to consider the gravitational force acting upon the plunger. Both the mechanical and electrical aspects of the motor modeling are analyzed. The mechanical equations are based on the summation of the applied forces to the plunger. The mechanical equation for the whole electromagnetic system can be written as follows:

$$\sum f = m\,a = m\frac{d^2x}{dt^2}, \tag{22}$$

$$m\frac{d^2x}{dt^2} + d.\frac{dx}{dt} = f_m, \tag{23}$$

where m is the mass of the plunger, d is the damping coefficient that represents the plunger function, f_m is the magnetic force acting on the plunger, and x is the position of the center of the plunger.

The magnetic force, f_m, is expressed by the following equation:

$$f_m = 0.5i^2\frac{dL}{dx}. \tag{24}$$

For motor electrical analysis, it is necessary to verify the motor's behavior when it is supplied from a DC source. A simple circuit diagram for the linear reluctance motor under DC supply is shown in Figure 5.
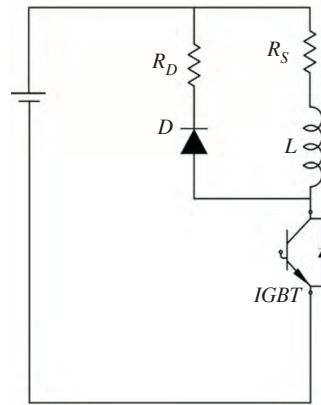
Figure 5. Diagram of the motor circuit connected to the DC source [14].

When the insulated gate bipolar transistor (IGBT) is turned on, the full voltage appears across the motor and the inductance of the coil windings causes the current to flow through the coil. When the IGBT is turned off, the energy stored in the inductance of the motor windings forces the diode into conduction. During this time, the current is decreasing. The electrical equations for the whole electromagnetic system when supplied from a DC source can be written as given below.

$$\frac{d\lambda}{dt} + i.R_S = V_S \tag{25}$$

$$\lambda = L(x).i = L.i \quad \Rightarrow \quad \frac{d\lambda}{dt} = L\frac{di}{dt} + i\frac{dL}{dx}.\frac{dx}{dt} \tag{26}$$

$$L\frac{di}{dt} + i\frac{dL}{dx}.\frac{dx}{dt} + i.R_S = V_S \tag{27}$$

Here, V_s is the DC voltage applied, R_S is the coil resistance, i is the coil current, and L is the coil inductance, which depends on the position of the plunger.

There are 2 modes of operation under DC supply, closed switch and open switch. The electrical equations for the closed and open switch modes of operation are presented in Eqs. (28) and (29), respectively.

$$L\frac{di}{dt} + i\frac{dL}{dx}.\frac{dx}{dt} + i.R_S = V_S \tag{28}$$

$$L\frac{di}{dt} + i\frac{dL}{dx}.\frac{dx}{dt} + i.(R_S + R_D) = 0 \tag{29}$$

R_D is an external resistor that is intended to damp the current of the inductor to 0, i.e. to damp the inductor energy rapidly. Eqs. (23), (28), and (29) can be solved numerically using the PC-MATLAB software package. In order to be solvable with PC-MATLAB, they must be transformed to the forms given below.

For the mechanical system:

$$x^{..} = \frac{(0.5L_d i^2 - dx^{.})}{m}. \tag{30}$$

For the electric circuit, when the switch is closed:

$$i^{\bullet} = \frac{V_S - L_d i .x^{\bullet} - iR_S}{L}. \tag{31}$$

When the switch is open:

$$i^{\bullet} = \frac{-L_d i .x^{\bullet} - i(R_S + R_D)}{L}. \tag{32}$$

Here,

$$L_d = \frac{dL}{dx}. \tag{33}$$

As the step winding consists of 3 defined parts, in the above equations, the inductance value must be proportional to the plunger position in each part. In other words, it is necessary to model the motor in 6 regions of operation. Three of these 6 regions describe the system when the plunger enters the coil and the 3 remaining regions describe the system while the plunger leaves the coil.

5. Performance characteristics of the step winding motor

In the motor structure, a smaller air gap between the plunger and winding results in better motor output characteristics. However, the air gap cannot be less than 2 mm because of mechanical limitations. Accordingly, all of the analyses are based on the assumption of a constant average air gap. For evaluating the operation improvement of the TLRM with the proposed step winding, 2 motors with the characteristics shown in Table 1 are compared with each other.

The detailed parameters of the proposed step winding motor are shown in Table 2.

Figure 6 shows the inductance curve of the TLRM with the step winding parameters shown in Table 2.

In order to prove the correctness of Figure 6, some points such as the maximum and minimum inductance ($L_{min} = 0.0028$ H and $L_{max} = 0.0079$ H) of the step winding motor can be compared with those listed in Table 2.

As shown in Figure 6, due to the utilization of step winding, the slope of the inductance curve is high at the beginning of the curve. This leads to a higher force at the beginning of the plunger movement, which can be considered as an initial velocity for the plunger.

The motor behavior under DC supply depends strongly on the position of the switch-on and switch-off sensors. The coil should be always switched on when the plunger is at the maximum swing in order to get the best motor performance, and it should be switched off before the center of the plunger reaches the coil center. After switching off, the coil current drops to 0 with a time constant; this depends on the coil resistance R_S,

R_D, and coil inductance $L(x)$. At the starting point of the simulation, when the motor starts working, the plunger is positioned at a distance of 0.175 m from the center of the coil (x = 0.175 m). A set of data was obtained for the motor energized from a 50-V DC source. In respect to the circuit in Figure 5, Figure 7 shows the coil currents for both motors.

**Table 1.** Parameters of the step and level winding motors used in the experiment and simulation.

Symbol	Quantity	Level winding	Step winding
N	Number of turns	702	702
D_{ci}	Coil inner diameter (mm)	20	20
D_{co}	Coil outer diameter (mm)	44	-
D_{po}	Plunger outer diameter (mm)	16	16
m	Mass of the plunger (kg)	0.27	0.27
d	Damping coefficient (N s/m)	1.03	1.03
L_c	Length of plunger (mm)	200	200
L_w	Length of winding (mm)	200	200
μ_{rc}	Relative magnetic permeability	385	385
r	Resistance coil (Ω)	0.82	0.91
d_c	Conductor diameter (mm)	1.6	1.6
$L_{\min}$	Minimum inductance (H)	0.0017	-
$L_{\max}$	Maximum inductance (H)	0.0068	-

Table 2. Detailed parameters of step winding motor.

Symbol	First virtual winding	Second virtual winding	Third virtual winding
N	390	234	78
$L_{min_{(H)}}$	0.0021	5.13e-4	3.87e-5
$L_{\max_{(H)}}$	0.0055	0.002	4.1e-4
D_{ci}	20	20	20
D_{co}	80	44	28
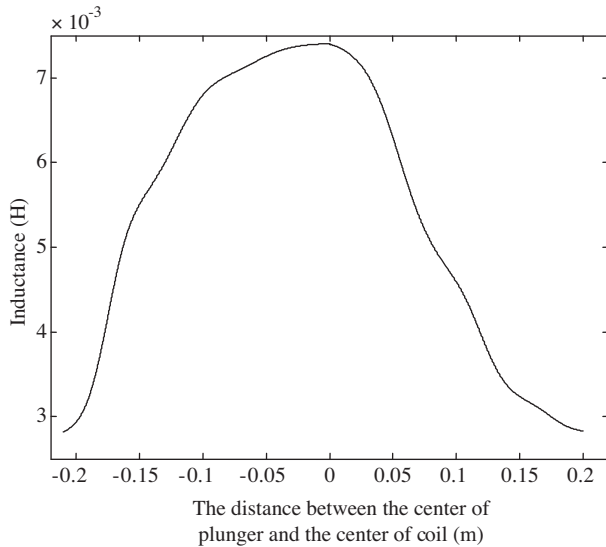
**Figure 6.** Inductance wave form of the step winding motor.
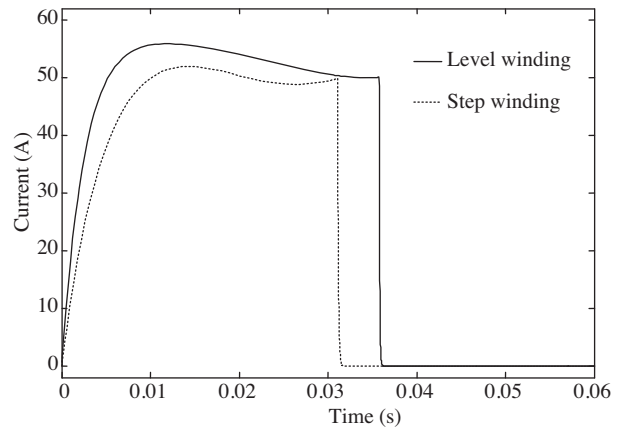
Figure 7. Simulation results of the coil current for 2 types of TLRM.

In the initial stages, the rising behavior of the current is like that of the air-core inductor, since the plunger has not yet moved very far in to the coil. After a few milliseconds, the current then begins to be limited by the circuit series resistance. At this point, the plunger moves into the bore of the coil and the value of the coil inductance increases, which limits the increase of the coil current. Before the plunger begins to exit the coil, the IGBT is switched off. Therefore, the coil current experiences an initial steep decay as the field energy is dissipated in the quenching resistor and circuit losses. When the switch is open and the plunger is moving out of the winding, if there is still any current flowing in the coil, the plunger will experience a retarding force, which returns energy to the magnetic field from the armature kinetic energy. Hence, it is necessary that coil's current drops to 0 immediately. It should be mentioned that $R_D = 80 \ \Omega$ in Figure 5.

In Figure 7, the average current drawn in the step winding motor is less than in the level winding motor. Moreover, the pulse duration is less in the step winding motor, which leads us to conclude that the plunger leaves the coil faster in the step winding motor than in the level winding motor. Thus, with less power consumption in the step winding motor, the plunger velocity is higher. For further illustration, the movement curve and duration of the plunger transmission are discussed further. Figure 8 represents the plunger movement curve in both motors.

At the beginning, the plunger position for the 2 motors is exactly same. In Figure 8, the duration of time it takes for the center of the plunger to reach the coil center is 0.031 s for the step winding motor and 0.036 s for the level winding motor. It is clear that the plunger moves faster in the step winding motor. The pulse duration was adjusted for maximum force and exit velocity for each motor.
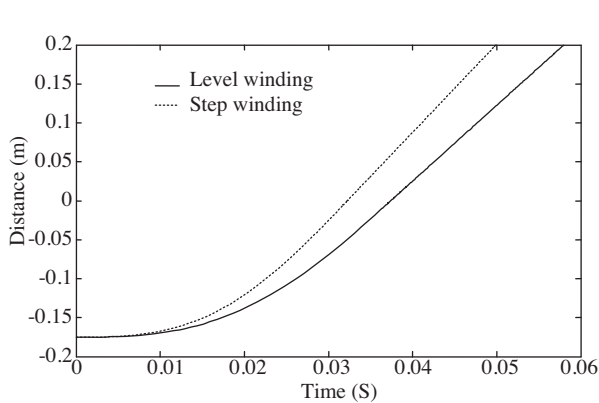
Figure 8. Comparison of the plunger trajectory for 2 types of TLRM.
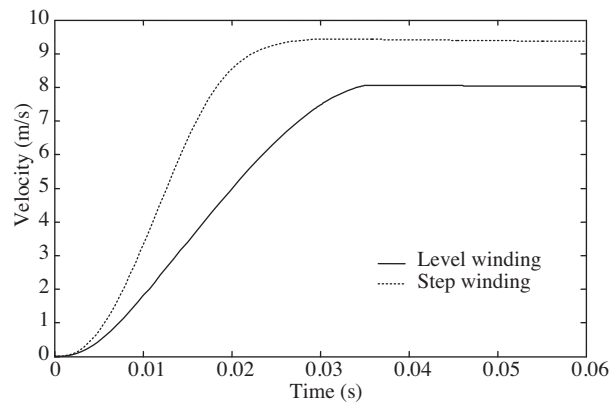
**Figure 9.** Comparison of the plunger velocity for 2 types of TLRM.

The windings of both motors are connected to the source before the plunger reaches the middle of the winding; meanwhile, the velocity of the plunger increases until it reaches its maximum velocity. At this time, the plunger is completely inside of the winding and the inductance is at its maximum. Simultaneously, the source must be disconnected; otherwise, the force generated reduces the plunger's speed and prevents it from exiting the coil. Figure 9 shows the plunger velocity in both motors.

In Figure 9, the plunger maximum velocity is 9.4 m/s in the step winding motor and 8.2 m/s in the level winding motor. As the plunger moves faster in the step winding motor, its pulse duration is less than that in the level winding motor, which leads to a reduction in the energy delivered to the motor. In other words, efficiency is increased. Our step winding motor has 3 winding parts. All of these parts play a role in producing force and velocity. The force produced by each part is shown in Figure 10.

The highest force is generated in the first step winding because the difference between the minimum and maximum inductance is the greatest; therefore, the inductance curve slope is the highest. In this motor, the total force applied to the plunger is the combination of forces applied to it in these 3 different winding parts. Figure 11 shows the generated force in both the step winding and level winding motors.
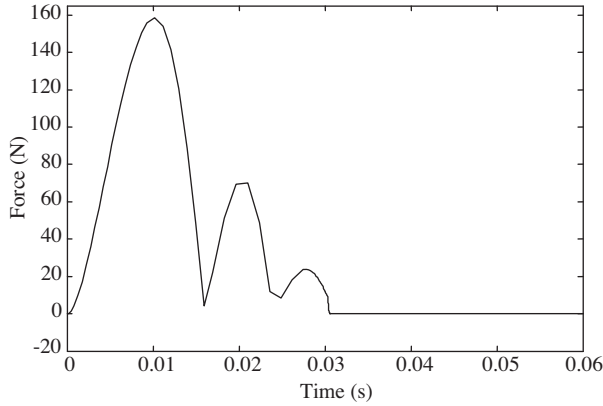
Figure 10. Comparison of the armature pressure (force) for the 3 separate virtual windings of the step winding motor.
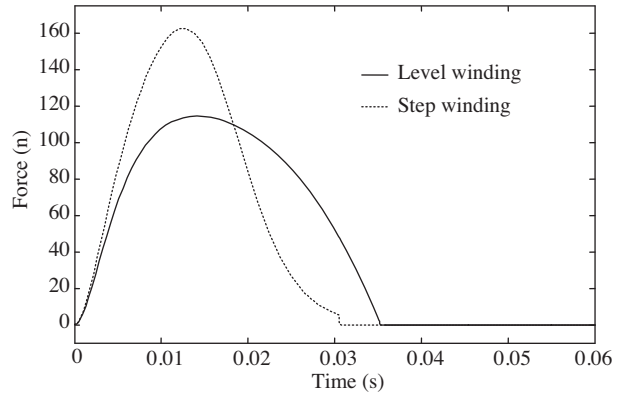
Figure 11. Comparison of the plunger pressure (force) for 2 types of TLRM.

As the force is proportional to the square of the coil current, and as the level winding TLRM draws more current from the source, it was expected that the level winding TLRM produces more force in comparison with the step winding motor. However, according to Figure 11, it is obvious that the latter produces more force than the former, which is due to the step winding motor structure.

The evaluation of the motor performance can be done via a calculation of efficiency. Efficiency is calculated using the following equation:

$$\eta = \frac{P_m}{P_{in}} \times 100. \tag{34}$$

Efficiency is one of the several important parameters that characterize the performance of a motor. To determine the efficiency of this particular motor when it operates in transient conditions, it is necessary to calculate the mean power by a numerical integration of the power waveform over one cycle. The efficiency of the level winding motor, when it is supplied from a 50-V source, is equal to 9%, while it reaches 11.8% in the step winding motor. Generally speaking, TLRMs do not have high efficiencies, as the air gap in these motors is larger than in other motors. However, in our case, the efficiency is low because the supplied voltage is low. If the motor is supplied from a 200-V DC source, efficiency in the level winding motor reaches 14.1%, while it reaches 17.95% in the step winding motor. When the voltage is increased, the current is increased; consequently, the force and the velocity, and accordingly the output mechanical power, all increase. Therefore, the plunger reaches the end of the coil faster, and the pulse width consequently decreases. The decreasing pulse width results in a decrease in the input power. Generally, the efficiency is increased.

6. Proposed structure validation

In this section, the method used for the inductance calculation and modeling is validated by the experimental results. Furthermore, to prove that the proposed structure generates more force than the usual TLRMs, FEM analysis is applied.

6.1. Experimental results

A small coil launcher was constructed (shown in Figure 12) for the purpose of verifying the numerical model. Measurements of coil current and exit velocity were carried out. A TLRM with the proposed step winding is shown in Figure 12.

Figure 12. Illustration of the step winding motor used in the experiments.
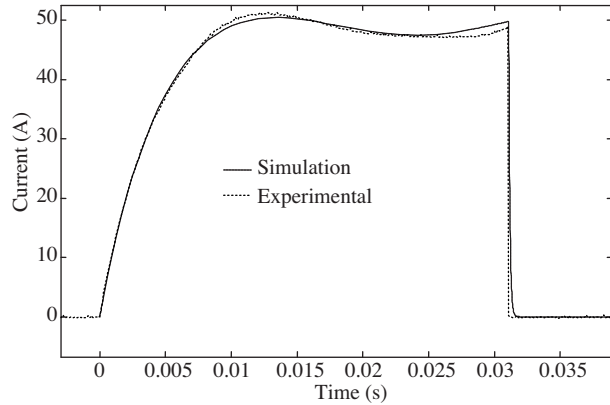

Figure 13. Comparison of a simulation with the experimental results of the coil current during the firing sequence.

The motor shown in Figure 12 is fed from a 50-V DC source. When feeding the motor with a 50-V DC source, the plunger leaves the coil with a velocity approximately equal to 9.3 m/s, which verifies the simulation results shown in the Figure. The light gate method is used to measure the velocity of the plunger. Figure 13 compares the motor current drawn from the experimental and simulation results.

In Figure 13, the 2 currents have very little difference, which confirms the accuracy of the modeling and the method used for the inductance calculation in the proposed motor.

6.2. FEM analysis

In order to validate the proposed motor, both the level winding and step winding motor structures are simulated, and the force generated in each one is calculated using FEM analysis. The forces applied to the plunger in both motors are shown in Figure 14.
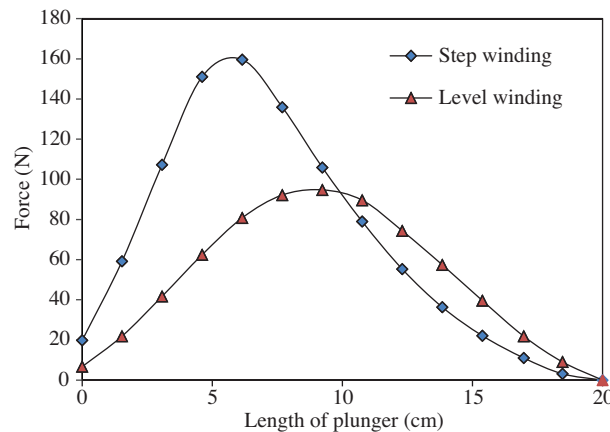
Figure 14. Comparison of the plunger pressure (force) for 2 types of TLRM using the FEM.

It must be mentioned that the winding current is constant and is the same for both motors. In other words, we assume that the motors are connected to a current-type source. In Figure 14, it is clear that the force generated in the step winding motor is more than that generated in the level winding motor. The step winding motor, which is implemented in 3D-FEM, is shown in Figure 15.
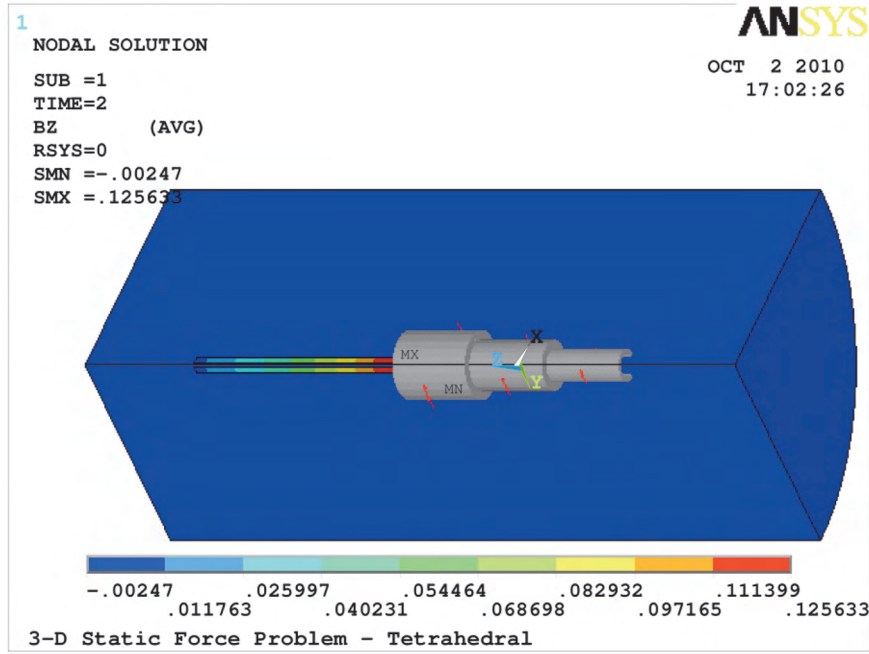

Figure 15. The magnetic field of the step winding when the plunger is at the beginning.

In Figure 15, the plunger is at the beginning of the winding and begins moving as the voltage is applied.

7. Conclusion

In this paper, a new structure for TLRMs is proposed, which has the same winding turns as a typical level winding TLRM. The proposed structure significantly improves the TLRM performance and generates more force and velocity. The experimental results show that even with less current being drawn from the source, this motor generates higher force and velocity. In other words, efficiency has improved in the proposed structure. This improvement is mainly because of the increasing of the slope of the inductance waveform at the beginning of the winding. Efficiency is considerably low in TLRMs due to a larger air gap in these motors, and it is highly dependent on the voltage applied to the motor. In fact, efficiency increases if the voltage applied to the proposed step winding motor in this paper increases. However, the voltage increase rate should not be so high as to prevent the current from increasing.

Comparing the experimental and simulation results allows an evaluation of the method used for the inductance calculation and motor modeling. Moreover, the FEM analysis proves that the proposed motor produces more force than typical TLRMs.

References

[1] S.A. Nasar, I. Boldea, Linear Electrical Motors: Theory, Design, and Practical Application, New Jersey, Prentice Hall, 1987.

[2] B. Marder, "A coilgun design primer", IEEE Transactions on Magnetics, Vol. 29, pp. 701-705, 1993.

[3] E.R. Laithwaite, A History of Linear Electrical Motors London Macmillan, pp. 31-59, 1987.

[4] J.J. Blakley, "A linear oscillating ferroresonant machine", IEEE Transactions on Magnetics, Vol. 19, pp. 1574-1579, 1983.

[5] S.A. Nasar, I. Boldea, Linear Electric Motors, New Jersey, Prentice Hall, 1987.

[6] T.J.E. Miller, "Optimal design of switch reluctance motors", IEEE Transactions on Industrial Electronics, Vol. 49, pp. 15-26, 2002.

[7] B. Tomczuk, M. Sobol, "Field analysis of the magnetic systems for tubular linear reluctance motors", IEEE Transactions on Magnetics, Vol. 41, pp. 1300-1305, 2005.

[8] E.A. Mendrela, "Comparison of the performance of a linear reluctance oscillating motor operating under AC supply with one under DC supply", IEEE Transactions on Energy Conversion, Vol. 14, pp. 328-332, 1999.

[9] D.A. Bresie, J.A. Andrews, "Design of a reluctance accelerator", IEEE Transactions on Magnetics, Vol. 27, pp. 623-627, 1991.

[10] E.A. Mendrela, Z.J. Pudlowski, "Transients and dynamics in a linear reluctance self-oscillating motor", IEEE Transactions on Energy Conversion, Vol. 7, pp. 183-191, 1992.

[11] J. Corda, S.M. Jamil, "Experimental determination of equivalentcircuit parameters of a tubular switched reluctance machine with solid-steel magnetic core", IEEE Transactions on Industrial Electronics, Vol. 57, pp. 304-310, 2010.

[12] Z.Q. Zhu, X. Chen, "Analysis of an E-core interior permanent magnet linear oscillating actuator", IEEE Transactions on Magnetics, Vol. 45, pp. 4384-4387, 2009.

[13] A. Waindok, G. Mazur, "A mathematical and physical models of the three-stage reluctance accelerator", IEEE 2nd International Students Conference on Electrodynamic and Mechatronics, pp. 29-30, 2009.

[14] S. Gibson, G.W. Jewell, R.E. Clark, "Variable-air gap, cylindrical, linear variable reluctance actuators for high-force, medium-stroke applications", IET Electric Power Applications, Vol. 3, pp. 352-362, 2009.

[15] B. Tomczuk, M. Sobol, "A field-network of a linear oscillating motor and its dynamics characteristics", IEEE Transactions on Magnetics, Vol. 41, pp. 2362-2367, 2005.

[16] AEV do Espírito Santo, MR Calado, CMP Cabrita, "Design and evaluation of a linear switched reluctance actuator for positioning tasks", Turkish Journal of Electrical Engineering and Computer Sciences, Vol. 18, pp. 925-941, 2010.